

On the effect of acoustic absorbers coupled to rocket combustors

Nancy Kings*[†] Alexander Chemnitz* Moritz Schulze* Thomas Sattelmayer*

*Lehrstuhl für Thermodynamik, Technische Universität München,

Boltzmannstr. 15, 85747 Garching, Germany

kings@td.mw.tum.de · chemnitz@td.mw.tum.de · schulze@td.mw.tum.de · sattelmayer@td.mw.tum.de

[†]Corresponding author

Abstract

The impact of an absorber ring coupled to a representative small-scale combustor-nozzle configuration under non-reactive ambient temperature conditions is investigated by experimental and numerical means. The combined approach serves for the identification of the system's eigenfrequencies, its mode shapes and the shielding effect caused by the dampers. The study reveals that tuning the cavity length of the quarter-wave resonators affects the acoustic pressure spectrum characteristics up- and downstream of the absorber ring. Downstream of the damping device two transverse mode structures are present while upstream of it solely one transverse mode occurs.

1. Introduction

Combustion chambers of rocket engines are often exposed to strong acoustical and vibrational loads caused by high-frequency (HF) combustion instabilities originating from flame-acoustic interaction. These constitute a risk for the rocket and its payload leading in the worst case to mission failure. Acoustic absorbers can be used to suppress the high energy oscillations originating from the first combustor transverse mode in order to achieve stable operating conditions. However, the influence of such damping devices coupled to the combustor on the acoustics is rather complex. The additional resonator volume changes the eigenfrequencies from that of pure cylinder modes. Furthermore, absorbers tuned to the first transverse mode frequency give rise to side peaks in the spectrum that were not present without damping devices. The knowledge of such complex acoustic interaction processes needs to be enhanced to improve absorber efficiency in rocket engines applications and prediction tools as well.

Experimental and numerical studies on the impact of single absorbers and absorber rings were conducted by Oschwald et al.⁶ and Schulze et al.⁸ A comprehensive literature review is given in Schulze et al.⁸ Grazing flow was not considered in the investigations. This is a drawback since grazing flow is likely present in rocket combustion chambers. Moreover, all conducted studies focussed on the acoustic field downstream of the absorber. The effect of the absorber ring on the acoustic field upstream of the damping device was not considered, although this might be decisive for the interaction between chamber and injector acoustics.

This work aims for a detailed investigation of the impact of an absorber ring coupled to a representative small-scale combustor-nozzle configuration under non-reactive ambient temperature conditions by experimental and numerical means. The combined approach serves for the identification of the system's eigenfrequencies, its mode shapes and the shielding effect caused by dampers. An absorber ring consisting of 20 quarter-wave tubes, equally distributed over the circumference, was integrated in a cold-flow combustor-nozzle configuration with a perforated plate at the inlet and a choked outlet. The absorber position relative to the combustor inlet was optimised for the detection of the acoustic field up- and downstream of the damping device by means of pressure sensor rings. By varying the cavity length of the quarter-wave tubes, their impact on the acoustics was modified.

In addition to the experiments, a CFD/CAA hybrid approach was used to determine mode shapes and eigenfrequencies of the different configurations. First, the mean flow quantities were derived from RANS simulations. Subsequently, the fluctuating quantities were obtained from acoustic simulations solving the Linearized Euler Equations (LEE) in frequency space. The changing reflection coefficient due to absorber length variations of each quarter-wave tube was mapped onto the corresponding combustor shell surface.

The experiments revealed that changing the cavity length of the quarter-wave tubes affects variably the acoustic pressure spectrum characteristics up- and downstream of the absorber ring. By means of the numerical analysis the

ON THE EFFECT OF ACOUSTIC ABSORBERS COUPLED TO ROCKET COMBUSTORS

system eigenfrequencies were identified and cross-checked with the experimentally detected main peaks. The comparison showed that the absorber ring generates acoustic modes restricted solely to the downstream combustor region. Moreover, transverse modes affecting the entire combustion chamber are present occurring at frequencies below the cut-on frequency of pure cylinder modes. The numerically predicted eigenfrequencies in dependence of amplitude and phase of the reflection coefficient have been studied and good agreement with the experimental data was found applying an analytical absorber model. The predicted mode shapes reveal the occurrence of a quasi-shielding effect due to the quarter-wave tubes. The frequency specific evaluation of the pressure data confirms the existence of modes shapes downstream of the damping device which are either evanescent or cut off upstream of it. Such different pressure spectrum characteristics up- and downstream of absorber rings needs to be considered for determining damping rates and for stability assessment tools in rocket engine design.

2. Test rig

The test rig consists of an air supply system, an injection head, a cylindrical chamber with a diameter of 92 mm and a length of 239 mm as well as a nozzle with an area ratio of 0.425 at its exit. The chamber comprises an absorber ring element and measurement sections up- and downstream of it, see Fig. 1 (left). Flow direction is from bottom to top. As indicated in Figure 1, acoustic excitation within the test rig is realised either via siren or broadband flow noise.

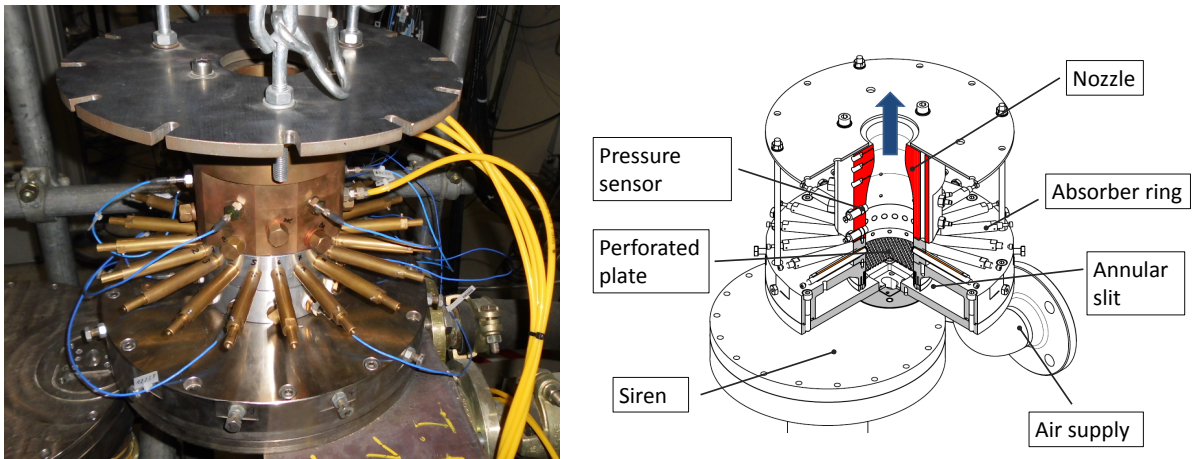


Figure 1: Test rig photo and sketch. Configuration with broadband flow noise (left) and siren excitation (right)

The small-scale combustor-nozzle configuration is operated at non-reactive ambient temperature conditions with pressurized air. At a mass flow rate of $\dot{m} = 1.15$ kg/s, the critical pressure ratio to establish choked nozzle flow conditions is reached yielding a Mach number of $M_c = 0.25$ and a static pressure of $p_c = 1.65$ bar in the chamber. To imitate the face plate with injection head of conventional rocket combustors, a perforated plate with high-bias flow and an open area ratio of 51% is used. The Mach number in the 3 mm holes is ≈ 0.4 .

A thin annular slit upstream of the injection head provides sonic conditions for the air inflow to decouple the chamber acoustics from the supply system. At the outlet of the small-scale combustor-nozzle configuration the choked flow condition in the nozzle throat decouples the chamber acoustics likewise from the environment further downstream. This isolates the acoustics of the system under consideration from the environment and leads to well-defined boundary conditions.

The absorber ring under investigation comprises 20 structurally identical cavities that are homogeneously distributed across the circumference and perpendicularly arranged to the combustion chamber wall. All cavities have a diameter of 8 mm and a variable length. The absorber ring element is located 76 mm downstream of the perforated plate. Two pressure sensor rings integrated in the measurement sections are used to study the pressure field 40 mm upstream and 73 mm downstream of the absorber ring element. Each pressure sensor ring comprises 6 dynamic pressure sensors of type PCB M1006B equally distributed in circumferential direction. The test rig specifications are given in Table 1.

2.1 Measurement strategy and experimental data evaluation

In the measurement campaign broadband excitation originating from flow noise was used to determine the eigenfrequencies of the combustor-nozzle configurations. The high-Mach number flow through the holes of the perforated plate

Table 1: Test rig specifications

Parameter	Symbol	Value
Chamber diameter	D_c	92 mm
Chamber length	L_c	147 mm
Chamber Mach number	M_c	0.25
Chamber pressure (static)	p_c	1.65 bar
Nozzle throat diameter	D_n	60 mm
Distance perforated plate to absorber ring	L_{P-A}	76 mm
Distance pressure sensor ring -upstream- to absorber ring	L_{up-A}	40 mm
Distance pressure sensor ring -downstream- to absorber ring	L_{do-A}	73 mm
Mass flow rate (pressurized air)	\dot{m}	1.15 kg/s
Absorber cavity length	L_A	35 mm
Theoretical optimal cavity length	$L_{A,th}$	39.24 mm
Absorber diameter	D_A	8 mm
Perforated plate, hole diameter	D_p	3 mm
Perforated plate, thickness	b_p	2 mm
Perforated plate, area ratio		51 %
Perforated plate, hole Mach number	M_p	0.4

represents an efficient broadband noise source providing a sufficient acoustic signal-to-noise ratio for the investigations. Such broadband excitation does not inherently alter the system eigenfrequencies.

The impact of the absorber ring with grazing flow on the chamber acoustics was determined by conducting measurements with the cavity length set to zero and to 35 mm. In the first case, no interaction of the absorber ring with the chamber acoustics occurs. When the cavity length is set to 35 mm all cavities of the absorber ring suppress the first transverse mode T_1 . The cavity length in the experiment is rather close to the theoretical optimum $L_{A,th}$ according to:

$$L_{A,th} = \frac{c}{4f_c} = \frac{\pi}{2 s_{10}} D_c/2 \approx 0.853 D_c/2 \Rightarrow L_{A,th} = 39.24 \text{ mm} \quad (1)$$

Here, f_c denotes the eigenfrequency of the first transverse mode of the chamber, $D_c/2$ the chamber radius and c the speed of sound. s_{10} is the zeroth root of the first-order Bessel function derivative.

Since the research focus was on transverse modes, the acoustic field was scanned by two pressure sensors rings, each equipped with 6 PCBs. 12 pressure signals were recorded simultaneously for a measurement duration of 1 s at a sampling frequency of 32 768 Hz and evaluated by cross-spectra analysis applying Hanning window function. To ensure accuracy of the experimental results, data of altogether 10 measurements were evaluated showing peaks at identical characteristic frequencies. For the chosen operating conditions the chamber provides reproducible acoustics.

3. Numerical setup

For the numerical study of the chamber acoustics, eigensolutions of the isentropic linearized Euler equation (LEE) in frequency space are obtained with a finite element approach. The equations are implemented in their weak form and discretized with elements of quadratic order. For stabilization a Galerkin/Least-Squares (GLS) approach is used. In the following, the governing equations are outlined before the boundary conditions and the computational grid are specified.

3.1 Governing equations

The LEE describe perturbations in a frictionless flow, based of the decomposition of a quantity ϕ into its mean and fluctuating part:

$$\phi = \bar{\phi} + \phi' \quad (2)$$

The LEE are solved in radial coordinates (r, θ, x) without swirl, i.e. zero azimuthal velocity, $u_\theta = 0$. The mean flow is modeled as rotational symmetric, corresponding to $\partial \bar{\phi} / \partial \theta = 0$. The fluctuating quantities are time harmonic, i.e.

$$\phi' = \hat{\phi} e^{i\Omega t} \quad (3)$$

ON THE EFFECT OF ACOUSTIC ABSORBERS COUPLED TO ROCKET COMBUSTORS

with the complex angular frequency Ω being composed of the angular eigenfrequency ω and the damping rate α :

$$\Omega = \omega + i\alpha \quad . \quad (4)$$

Due to the isentropy of the fluctuating fields, pressure fluctuations can be related to density fluctuations ρ' via the sound speed c :

$$p' = c^2 \rho' \quad . \quad (5)$$

Under these conditions the continuity equation reads

$$i\Omega\hat{\rho} + \hat{u}_r \left(\frac{\partial \bar{\rho}}{\partial r} + \frac{1}{r} \bar{\rho} \right) + \hat{u}_x \frac{\partial \bar{\rho}}{\partial x} + \bar{\rho} \left(\frac{\partial \bar{u}_r}{\partial r} + \frac{1}{r} \bar{u}_r + \frac{\partial \bar{u}_x}{\partial x} \right) + \bar{\rho} \frac{\partial}{\partial r} \hat{u}_r + \bar{\rho} \frac{\partial}{\partial x} \hat{u}_x + \bar{u}_x \frac{\partial}{\partial x} \hat{\rho} + \bar{u}_r \frac{\partial}{\partial r} \hat{\rho} + \bar{\rho} \frac{1}{r} \frac{\partial}{\partial \theta} \hat{u}_\theta = 0 \quad . \quad (6)$$

The momentum equation in r , θ and x direction respectively reads

$$\begin{aligned} i\Omega\hat{u}_r + \hat{u}_r \frac{\partial \bar{u}_r}{\partial r} + \hat{u}_x \frac{\partial \bar{u}_r}{\partial x} - \hat{\rho} \frac{1}{\bar{\rho}^2} \frac{\partial \bar{p}}{\partial r} + \bar{u}_r \frac{\partial \hat{u}_r}{\partial r} + \bar{u}_x \frac{\partial \hat{u}_r}{\partial x} + \frac{c^2}{\bar{\rho}} \frac{\partial \hat{\rho}}{\partial r} &= 0 \\ i\Omega\hat{u}_\theta + \hat{u}_\theta \frac{\bar{u}_r}{r} + \bar{u}_r \frac{\partial \hat{u}_\theta}{\partial r} + \bar{u}_x \frac{\partial \hat{u}_\theta}{\partial x} + \frac{c^2}{\bar{\rho} r} \frac{\partial \hat{\rho}}{\partial \theta} &= 0 \\ i\Omega\hat{u}_x + \hat{u}_r \frac{\partial \bar{u}_x}{\partial r} + \hat{u}_x \frac{\partial \bar{u}_x}{\partial x} - \hat{\rho} \frac{1}{\bar{\rho}^2} \frac{\partial \bar{p}}{\partial x} + \bar{u}_r \frac{\partial \hat{u}_x}{\partial r} + \bar{u}_x \frac{\partial \hat{u}_x}{\partial x} + \frac{c^2}{\bar{\rho}} \frac{\partial \hat{\rho}}{\partial x} &= 0 \quad . \end{aligned} \quad (7)$$

To reduce the computational effort, the simulations are carried out in the r - x -plane and the azimuthal dependence of the complex amplitude distribution is modeled following Mensah and Moeck⁵ as

$$\hat{\phi} = \tilde{\phi} e^{i\theta} \quad . \quad (8)$$

3.2 Boundary conditions and computational grid

The mean flow is modeled as quasi-one dimensional. Effects of the components upstream of the perforated plate as well as the flow stratification present in the injection region are accounted for via a reflection coefficient boundary condition at the inlet. The reflection coefficient⁷ has been determined based on experimental data from Kathan.² Since the flow at the nozzle end is supersonic a non-reflecting boundary condition was used in the nozzle throat. Absorbers are modeled via a reflection coefficient as described in the next section.

The computational grid used has 130 188 degrees of freedom with a resolution of 280 (axial) x 28 (radial) elements.

3.3 Absorber modeling

As proposed in Cardenas¹ and Schulze,⁷ the absorber ring is modeled as a reflection coefficient boundary condition applied to a continuous shell surface replacing the absorber ring. Its reflection coefficient R_A is calculated from that of a single absorber R_{SA} by

$$R_A = \frac{A_A Z_{SA} - N_{SA} A_{SA}}{A_A Z_{SA} + N_{SA} A_{SA}} \quad (9)$$

where Z_{SA} is the single absorber impedance, A_A the area of the absorber shell, A_{SA} the cross sectional area of a single absorber and N_{SA} the number of absorbers in the ring. In this study, the height of the shell surface corresponds to the absorber diameter.

The determination of the single absorber impedance is associated with a certain degree of uncertainty. Several analytical models are available. In Schulze⁷ an analytic model from Laudien et al.³ has been used to model the single absorber impedance:

$$Z_{SA} = \frac{2}{\bar{\rho} c} \left(\epsilon_l + \epsilon_{nl} + \frac{l_a}{d_a} \right) \sqrt{\mu \bar{\rho} \omega} - i \cot \left(\frac{l_e \omega}{c} \right) \quad (10)$$

Here, d_a and l_a are the geometric diameter and length of the absorber respectively and μ the dynamic viscosity. ϵ represents the linear damping effect of the absorber, ϵ_{nl} nonlinear effects and l_e is an effective absorber length representing inertia effects. In Laudien et al.³ it is shown experimentally that for quarter-wave tubes nonlinearities are of minor

ON THE EFFECT OF ACOUSTIC ABSORBERS COUPLED TO ROCKET COMBUSTORS

importance, i.e. $\epsilon_l + \epsilon_{nl} \approx \epsilon_l$. However, no procedure for evaluating ϵ_l is provided. Cardenas¹ derived an approach similar to equation (10):

$$Z_{SA} = \frac{2}{\bar{\rho}c} \left(1 + \epsilon_{nl} + \frac{l_r}{d_a} \right) \sqrt{\mu\bar{\rho}\omega} - i \cot\left(\frac{l_e\omega}{c}\right) \quad (11)$$

with $l_r \approx 0.405l_a - 0.08d_a$. In Schulze,⁷ $\epsilon_l = 1$ has been used including non-linear effects.

For the length correction different values can be found as well. While in the work of Schulze⁷ $l_e - l_a = \frac{4}{3\pi}d_a$ is used, Levine and Schwinger⁴ proposed $l_e - l_a = 0.6133d_a$ that provided good results in the studies of Soto-Nicolas.⁹

Apparently, all three model parameters of the real part of the impedance are associated with a relatively high degree of uncertainty. Thus, a parametric study is conducted in Section 5.1 for a combined parameter ϵ_{tot} for an equation of the form

$$Z_{SA} = \frac{2}{\bar{\rho}c} \epsilon_{tot} \sqrt{\mu\bar{\rho}\omega} - i \cot\left(\frac{l_e\omega}{c}\right) \quad (12)$$

4. Experimental results

For the characterization of the acoustic sound field up- and downstream of the absorber ring the dominant eigenfrequencies are determined without dampers (reference case) and with tuning the 20 cavities of the absorber ring to the first transverse mode T_1 .

4.1 Identification of dominant eigenfrequencies in the chamber

The cross-spectra between pressure sensors up- and downstream of the absorber ring for different circumferential positions are given in Figure 2. For the reference case, a distinct peak at $f = 2080$ Hz and a weaker amplitude maximum at $f = 2239$ Hz indicate two governing modes in the frequency range up to 3000 Hz.

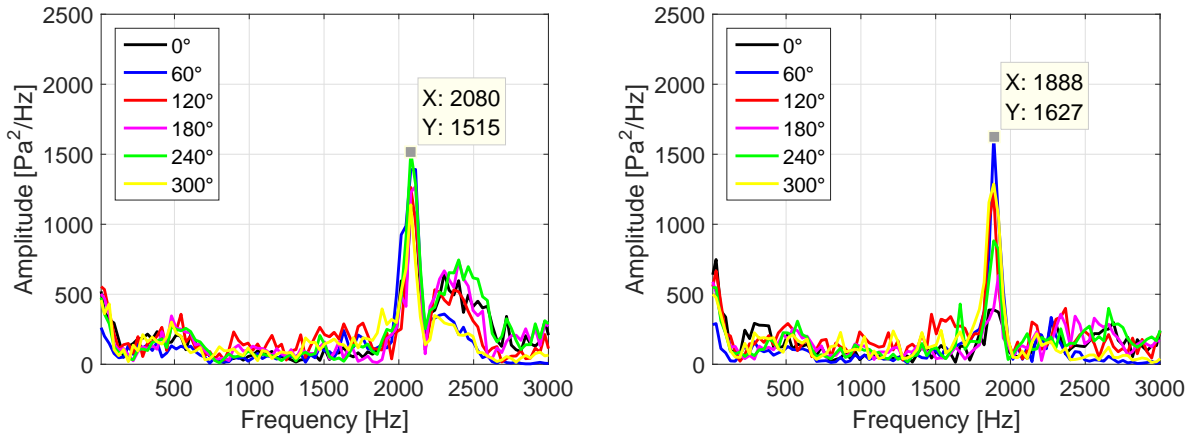


Figure 2: Cross-spectra without (left) and with absorber (right): evaluation of pressure signals up- and downstream of the absorber ring across the chamber circumference

The distinct peak corresponds to the fundamental transverse mode ($1T$), which is close to the theoretical cut-on frequency of $f_{th-cut-on} = 2090$ Hz, see equation (13). Here, the small discrepancy results from the theoretical cut-on definition excluding complex boundary condition such as the in- and outlet of the test rig. The second frequency at $f = 2239$ Hz corresponds to the first transverse mode combined with the first longitudinal mode ($1T1L$).

$$f_{th-cut-on} = \frac{cS_{10}}{R_C} \sqrt{1 - M_c^2} \quad (13)$$

When the absorber cavities are tuned to suppress the first transverse mode T_1 at $f = 2080$ Hz, high acoustic velocities establish in case of resonance conditions within the cavities and maximum acoustic dissipation occurs. The corresponding cross spectra of the pressure sensors up- and downstream are shown in Figure 2 (right). Within the

ON THE EFFECT OF ACOUSTIC ABSORBERS COUPLED TO ROCKET COMBUSTORS

combustion chamber the governing mode is shifted to a lower frequency at $f = 1888$ Hz that is present in the entire chamber.

4.2 Spatial identification of tangential mode shapes

For the identification of the spatial shapes of the tangential modes up- and downstream of the absorber ring, the pressure signals detected by opposing PCB-sensors (180 degree phase offset) at each pressure sensor ring were cross-checked. The cross-spectrum yielding the maximum amplitude value of the transverse mode structure is plotted, see Figure 3.

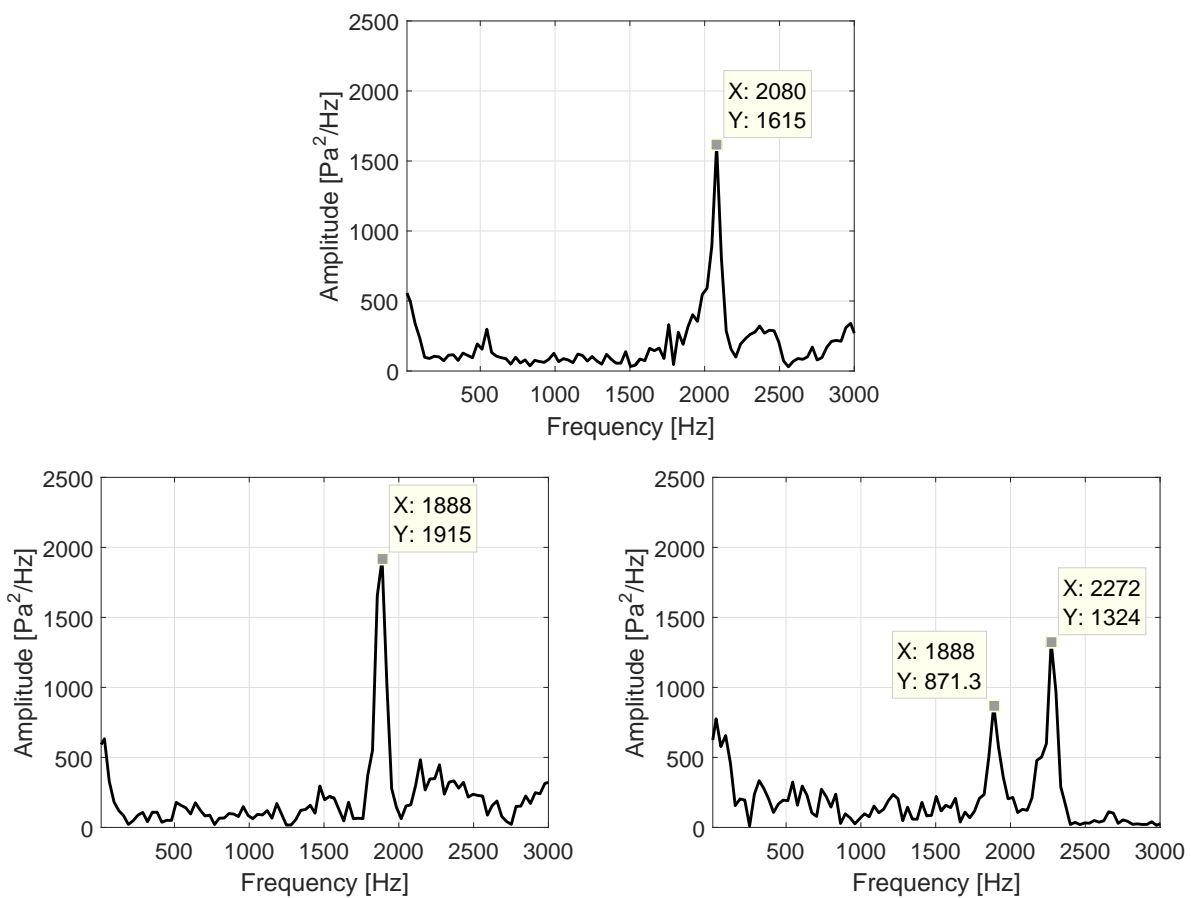


Figure 3: Cross-spectra without (top) and with absorbers (bottom). Bottom left: Pressure sensor ring upstream of the absorber ring, transverse mode T_1^- . Bottom right: Pressure sensor ring downstream of the absorber ring transverse modes T_1^- and T_1^+

In the reference case the cross-spectrum derived from the evaluation of the pressure ring resemble the spectrum shown in Figure 2 (left) since the transverse mode expands over the entire chamber. When the resonator cavity length is tuned to the first transverse mode T_1 upstream of the damping device only the peak of the transverse mode at $f = 1888$ Hz is detected, denoted here as T_1^- . In contrast, downstream of the absorber ring two transverse modes are visible, one at $f = 1888$ Hz and the other at $f = 2272$ Hz. The lower transverse mode corresponds to the chamber mode T_1^- affecting the entire chamber. The second transverse mode structure is found solely downstream of the absorber ring and is denoted here as T_1^+ . Consequently, it can be concluded that the absorber ring spatially decouple the T_1^+ mode from the faceplate and the chamber acoustics concentrates to the rear part of the combustion chamber. However, the transverse mode T_1^- affects the entire chamber, occurs at a frequency below the cut-on frequency of the pure cylinder mode and might be able to interact with faceplate or injector acoustics.

5. Numerical Results

The comparison of the numerical results to the experimental data is based on the eigenfrequencies. As outlined before, the T_1^- mode is located at a frequency below the cut-on frequency. This implies that the absorber ring must provide an effective increase of the radial cross-section beyond that of the chamber allowing for the presence of a transverse mode below the cylindrical chamber's cut-on frequency.

5.1 Absorber ring reflection coefficient

The numerical calculations provide the mode structure inside the chamber. To address the uncertainty in the absorber modeling, absolute value and phase of the absorber impedance were varied systematically. The range of both parameters was chosen based on the reflection coefficient calculated from equation (12). Thereby ϵ_{tot} is varied between 1, corresponding to a conservative lower limit of equations (10) and (11), and $\epsilon_{tot} = 21$, approximately reproducing the absorber ring reflection coefficient from Schulze.⁷ For the length correction, the approach already employed there ($l_e - l_a = \frac{4}{3\pi}d_a$) was used. The corresponding reflection coefficients are shown in Figure 4.

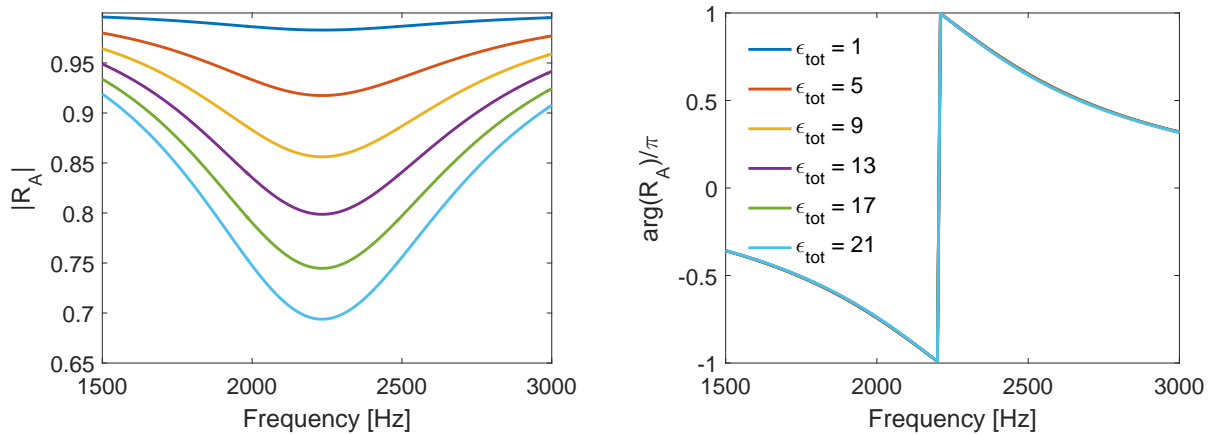


Figure 4: Absorber ring reflection coefficient for various values of ϵ_{tot} ; amplitude (left) and phase(right)

5.2 Eigenfrequencies

The computed eigenfrequencies for both, the T_1^- and T_1^+ mode are given in Figure 5. It can be seen that the obtained eigenfrequency is primarily depending on the phase of the absorber reflection coefficient. A slight influence of the reflection coefficient's absolute value is visible as well. However, as e.g. the iso-line of the experimental value in Figure 5 indicates, its effect on the eigenfrequency is non uniform with an increase of the reflection coefficient leading to an increase of eigenfrequency for the T_1^- but to a decrease for the T_1^+ mode.

The absorber models used in this study describe specific curves in the absolute value-phase-space, which are included in Figure 5. Each complex impedance corresponds to a certain frequency (cf. Figure 4). Thus, the value predicted for each absorber curve can be calculated as its intersection with the numerical eigenfrequency distribution in the reflection coefficient-frequency-space. The corresponding points are marked as white dots in Figure 5. For both eigenmodes the resulting eigenfrequencies match the experimental values well. This shows that the effective increase of the cross-sectional combustor area due to the absorber ring can be captured by the absorber impedance model. Comparing the reflection coefficients' phases for both modes a notable difference is visible with $arg(R_A) \approx -0.6\pi$ for the T_1^- and $arg(R_A) \approx -1.1\pi$ for the T_1^+ mode. This value is nearly constant for all values of ϵ_{tot} indicating a weak influence of this parameter on the predicted eigenfrequency.

ON THE EFFECT OF ACOUSTIC ABSORBERS COUPLED TO ROCKET COMBUSTORS

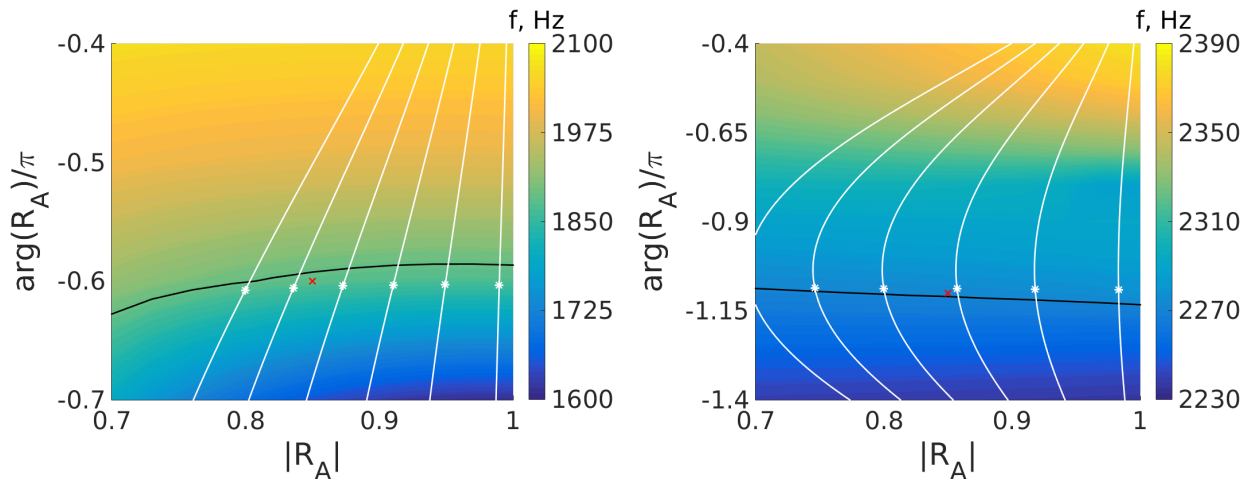


Figure 5: Eigenfrequencies of the T_1^- (left) and T_1^+ (right) eigenmodes; black: experimental value isoline; white lines: absorber model reflection coefficients from Figure 4; white points: frequency obtained with absorber model; red: parameters used for Figure 6

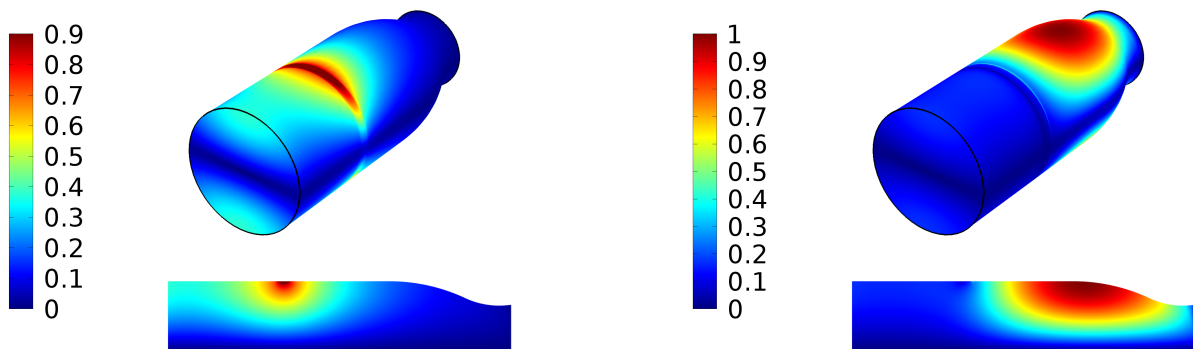


Figure 6: Normalized pressure distribution of the T_1^- (left) and the T_1^+ mode (right); top: 3D distribution; bottom: cut through pressure anti-nodal plane

5.3 Eigenmodes

The numerical results allow for the visualization of eigenmode shapes. In the study conducted on the reflection factor range an influence on the eigenmode shapes has been observed. Two values of the reflection coefficient have been chosen, whose eigenfrequencies lie close to the experimental values, marked red in Figure 5. The corresponding normalized pressure amplitude distributions are shown in Figure 6. For the T_1^- mode highest pressure amplitudes are present in the absorber region confirming the aforementioned anchoring of the mode in the absorber ring. However, notable pressure amplitudes are present up to the faceplate as well as downstream of the absorber. The decrease in the pressure amplitude towards the nozzle is higher than towards the faceplate. In contrast, the T_1^+ mode is located predominantly in the rear section of the chamber, downstream of the absorber, and extends through the convergent part of the nozzle. This matches the spatial separation of the modes by the absorber observed in the experiment.

6. Conclusions

The impact of an absorber ring on the system eigenfrequencies has been analyzed using flow noise excitation. It has been shown that tuning the resonator cavity length to suppress the first transverse mode generates two transverse mode structures T_1^- and T_1^+ downstream of the absorber ring visible as discrete peaks in the spectrum. Upstream of the damping device only the lower transverse mode T_1^- is present occurring at a frequency below the cut-on frequency

ON THE EFFECT OF ACOUSTIC ABSORBERS COUPLED TO ROCKET COMBUSTORS

of the pure cylinder mode. Consequently, only this mode is able to interact with faceplate or injector acoustics. In contrast, the absorber ring spatially decouples the T_1^+ mode from the faceplate and regions with high acoustic pressure are concentrated to the rear part of the combustion chamber.

A numerical eigensolution study of the test case has been carried out based on the LEE in frequency space with the absorbers modeled as an impedance boundary condition. The predicted eigenfrequencies in dependence of amplitude and phase of the reflection coefficient have been studied and good agreement with the experimental data can be reached with an analytical absorber model. Hereby the phase of the absorber impedance has been identified as the primary influencing parameter. For a fixed length correction the other absorber model parameters only exert a weak influence on the eigenfrequency.

In realistic rocket-engine combustors, absorber rings are placed close to the faceplate favorably near the region of strong interaction between acoustics and combustion process. The absorber ring impact yielding one transverse mode structure T_1^- that is able to interact with the injector and another transverse mode T_1^+ that is restricted to the region downstream of the absorber should be carefully addressed in the design process of combustion chambers.

7. Acknowledgments

The financial support from the German Research Foundation (DFG) in the framework of the Sonderforschungsbereich Transregio 40 for conducting this study is gratefully acknowledged.

References

- [1] M. A. Cárdenas. *Influence of Enhanced Heat Transfer in Pulsating Flow on the Damping Characteristics of Resonator Rings*. Dissertation, Technische Universität München, Munich, 2014.
- [2] R. Kathan. *Verlustmechanismen in Raketebrennkammern*. Phd thesis, Technische Universität München, Munich, 2013.
- [3] E. Laudien, R. Pongratz, R. Pierro, and D. Preclik. *Liquid Rocket Engine Combustion Instability, Progress in Astronautics and Aeronautics*, chapter Experimental Procedures Aiding the Design of Acoustic Cavities. AIAA, 1995.
- [4] H. Levine and J. Schwinger. On the Radiation of Sound from an Unflanged Circular Pipe. *Phys. Rev.*, 73:383–406, Feb 1948.
- [5] G. A. Mensah and J. P. Moeck. Efficient Computation of Thermoacoustic Modes in Annular Combustion Chambers Based on Bloch-Wave Theory. In *Turbo Expo: Power for Land, Sea, and Air*, volume 4B: Combustion, Fuels and Emissions. ASME, 2015.
- [6] M. Oswald, Z. Farago, G. Searby, and F. Cheuret. Resonance Frequencies and Damping of a Combustor acoustically coupled to an Absorber. *Journal of Propulsion and Power*, 24:524–533, 2008.
- [7] M. Schulze. *Linear Stability Assessment of Cryogenic Rocket Engines*. PhD thesis, Technische Universität München, Munich, 2016. <https://www.td.mw.tum.de/fileadmin/w00bso/www/Forschung/Dissertationen/schulze16.pdf>.
- [8] M. Schulze, R. Kathan, and T. Sattelmayer. Impact of Absorber Ring Position and Cavity Length on Acoustic Damping. *Journal of Spacecraft and Rockets*, 52:917–927, 2015.
- [9] A. Soto-Nicolas. Measurements on Quarterwavelength Tubes and Helmholtz Resonators. In *Acoustics'08 Paris*. Paris, 2008.